Mon. Not. R. Astron. Soc. **000**, 000–000 (0000) Printed 29 January 2022 (MN LATEX style file v2.2)

Improving the precision matrix for precision cosmology

Dante J. Paz[1,2] ⋆ and Ariel G. Sánchez[3]

[1] *Instituto de Astronomía Teórica y Experimental, UNC-CONICET, Córdoba, Argentina.*
[2] *Observatorio Astronómico de Córdoba, Universidad Nacional de Córdoba, Argentina.*
[3] *Max-Planck-Institut für extraterrestrische Physik, Postfach 1312, Giessenbachstr., 85741 Garching, Germany.*

arXiv:1508.03162v2 [astro-ph.CO] 28 Sep 2015

Submitted to MNRAS

ABSTRACT

The estimation of cosmological constraints from observations of the large scale structure of the Universe, such as the power spectrum or the correlation function, requires the knowledge of the inverse of the associated covariance matrix, namely the precision matrix, $\mathbf{\Psi}$. In most analyses, $\mathbf{\Psi}$ is estimated from a limited set of mock catalogues. Depending on how many mocks are used, this estimation has an associated error which must be propagated into the final cosmological constraints. For future surveys such as Euclid and DESI, the control of this additional uncertainty requires a prohibitively large number of mock catalogues. In this work we test a novel technique for the estimation of the precision matrix, the covariance tapering method, in the context of baryon acoustic oscillation measurements. Even though this technique was originally devised as a way to speed up maximum likelihood estimations, our results show that it also reduces the impact of noisy precision matrix estimates on the derived confidence intervals, without introducing biases on the target parameters. The application of this technique can help future surveys to reach their true constraining power using a significantly smaller number of mock catalogues.

Key words: large-scale structure of the Universe – methods: data analysis, observational, statistics

1 INTRODUCTION

The small statistical uncertainties associated with current cosmological observations allow for precise cosmological constraints to be derived (e.g. Anderson et al. 2014; Planck Collaboration et al. 2015). Future stage IV experiments such as Euclid (Laureijs et al. 2011) and the Dark Energy Spectroscopic Instrument (DESI Eisenstein & DESI Collaboration 2015) will push the attainable level of precision even further, providing a strong test of the standard ΛCDM cosmological model.

As statistical uncertainties are reduced, the control of potential systematic errors becomes essential to derive robust cosmological constraints. Besides the correct treatment of the observations and accurate models of the data, precision cosmology requires a thorough control of the assumptions made when establishing the link between theory and observations. For example, most analyses of clustering statistics assume a Gaussian likelihood function. This assumption must be carefully revised as they might introduce systematic biases on the obtained confidence levels (Kalus et al. 2015).

Even for the Gaussian case, the evaluation of the likelihood function requires the knowledge of the precision matrix, $\mathbf{\Psi}$, that is, the inverse of the covariance matrix of the measurements. In most analyses of clustering measurements, the precision matrix is estimated from an ensemble of mock catalogues reproducing the selection function of each survey (e.g. Manera et al. 2013, 2014). However, all estimates of $\mathbf{\Psi}$ based on a finite number of mock catalogues are affected by noise. A rigorous statistical analysis requires the propagation of these uncertainties into the final cosmological parameter constraints.

Recent studies have provided a clear description of the dependence of the noise in the estimated precision matrix on the number of mock catalogues used (Taylor, Joachimi, & Kitching 2013), its propagation to the derived parameter uncertainties (Dodelson & Schneider 2013; Taylor & Joachimi 2014) and the correct way to include this additional uncertainty in the obtained cosmological constraints (Percival et al. 2014). The results from these studies show that, depending on the number of bins of a given measurement, a large number of mock catalogues might be necessary in order to keep this additional source of uncertainty under control.

⋆ E-mail: dpaz@oac.unc.edu.ar

© 0000 RAS

For future large-volume surveys such as Euclid or DESI, this requirement might be infeasible, even if these are based on approximated methods such as PINOCCHIO (Monaco et al. 2002), COLA (Tassev et al. 2013; Koda et al. 2015), PATCHY (Kitaura et al. 2014) or EZMOCKS (Chuang et al. 2015) instead of full N-body simulations.

In this paper we test the implementation of the Covariance Tapering (CT) method (Kaufman, Schervish, & Nychka 2008) as a tool to minimize the impact of the noise in precision matrix estimates derived from a finite set of mock catalogues. Although this technique was originally designed as a way to speed-up the calculation of maximum likelihood estimates, we show that this method can also be used to reduce the noise in the estimates of the precision matrix. The covariance tapering approach can help to obtain parameter constraints that are close to ideal (i.e. those derived when the true covariance matrix is known) even when the precision matrix is estimated from a manageable number of realizations. Our results show that CT can significantly reduce the number of mock catalogues required for the analysis of future surveys, allowing these data to reach their full constraining power.

The structure of the paper is as follows. In Sec. 2 we summarize the results of previous works regarding the impact of the noise in precision matrix estimates on cosmological constraints. The CT technique is described in Sec. 3. In Sec. 4 we apply CT to the same test case studied by Percival et al. (2014), that of normally-distributed independent measurements of zero mean. We then extend this analysis to a case with non-zero intrinsic covariances. Section 5 presents a study of the applicability of CT to the measurement of the baryon acoustic oscillations (BAO) signal using Monte Carlo realizations of the of the large-scale two-point correlation function. Finally, in Sect. 6 we present our main conclusions.

2 IMPACT OF PRECISION MATRIX ERRORS ON COSMOLOGICAL CONSTRAINTS

In most cosmological analyses the information from observations is compressed into a measurement $\mathbf{D}$, such as the power spectrum or the correlation function. It is commonly assumed that this measurement is drawn from a multi-variate Gaussian distribution with a given mean $\langle\mathbf{D}\rangle$ and covariance matrix, $\mathbf{C}$. Following a Bayesian framework, the measurement $\mathbf{D}$ can be used to constrain a set of cosmological parameters $\boldsymbol{\theta}$ by means of an unbiased model $\mathbf{T}(\boldsymbol{\theta}) = \langle\mathbf{D}\rangle\,(\boldsymbol{\theta})$. In such way, the probability that the data vector $\mathbf{D}$ corresponds to a realization of the model $\mathbf{T}(\boldsymbol{\theta})$ is given by the likelihood function

$$\mathcal{L}(\mathbf{D}|\boldsymbol{\theta},\boldsymbol{\Psi}) \propto |\boldsymbol{\Psi}|^{1/2} \exp\left[-\frac{1}{2}\chi^2(\mathbf{D},\boldsymbol{\theta},\boldsymbol{\Psi})\right], \tag{1}$$

where χ^2 is a quadratic form

$$\chi^2 = \sum_{ij} \left(D_i - T_i\left(\boldsymbol{\theta}\right)\right) \Psi_{ij} \left(D_j - T_j\left(\boldsymbol{\theta}\right)\right), \tag{2}$$

and $\boldsymbol{\Psi}$ corresponds to the inverse of the covariance matrix $\mathbf{C}$, known as the precision matrix.

The evaluation of the likelihood function requires the knowledge of the precision matrix, which is commonly derived from a set of N_s independent synthetic measurements, $\mathbf{D}^k$, based on mock catalogues matching the properties of the real data. The covariance matrix of the sample can be inferred using the unbiased estimator

$$\hat{C}_{ij} = \frac{1}{N_\mathrm{s}-1}\sum_{k=1}^{N_\mathrm{s}}(D_i^k - \bar{D}_i)(D_j^k - \bar{D}_j), \tag{3}$$

where $\bar{D}_i = \frac{1}{N_\mathrm{s}}\sum_k D_i^k$ is the mean value of the measurements at the i-th bin, over the set of mock catalogues, which provides an unbiased estimate of the ensemble average $\langle\mathbf{D}\rangle$. When independent realizations are used, the statistics of the uncertainties in the covariance and precision matrices are governed by the Wishart and inverse-Whishart distributions (Wishart 1928), respectively. As the inverse-Whishart distribution is asymmetric, the inverse of $\hat{\mathbf{C}}$ given by equation (3) provides a biased estimate of the precision matrix. However, it is possible to correct for this bias simply by including a prefactor as (Kaufman 1967; Hartlap, Simon, & Schneider 2007)

$$\hat{\boldsymbol{\Psi}} = \left(1 - \frac{N_\mathrm{b}+1}{N_\mathrm{s}-1}\right)\hat{\mathbf{C}}^{-1}, \tag{4}$$

where N_b corresponds to the number of bins in the measurement $\mathbf{D}$.

As this approach is based on a finite number of realizations, the estimator in equation (4) will be affected by noise (Taylor et al. 2013), whose effect must be propagated into the obtained constraints on the target parameters. The accuracy of the obtained confidence levels on the parameters $\boldsymbol{\theta}$ and their respective covariances is then ultimately limited by the uncertainties in the estimated precision matrix $\hat{\boldsymbol{\Psi}}$ (Taylor & Joachimi 2014).

Dodelson & Schneider (2013) performed a detailed analysis of the impact of the uncertainties in $\hat{\Psi}$. They showed that, up to second order in the covariance errors, this additional uncertainty can be described by a rescaling of the parameter covariances $\langle\Delta\theta_i\Delta\theta_j\rangle$ by a factor

$$f = 1 + B\,(N_\mathrm{b} - N_\mathrm{p})\,, \tag{5}$$

where N_p corresponds to the number of parameters measured and

$$B = \frac{(N_\mathrm{s} - N_\mathrm{b} - 2)}{(N_\mathrm{s} - N_\mathrm{b} - 1)(N_\mathrm{s} - N_\mathrm{b} - 4)}. \tag{6}$$

However, as shown by Percival et al. (2014), the correction factor of equation (5) cannot be directly applied to the errors derived from maximum likelihood estimates (MLE) based on a given data set. The error in the precision matrix introduces a bias in the recovered parameter uncertainties, which then deviate from those of the ideal case in which the true covariance matrix is known. To take this fact into account, the parameter covariances recovered from the measurements $\mathbf{D}$ must be rescaled by a factor

$$g = \frac{1 + B(N_\mathrm{b} - N_\mathrm{p})}{1 + A + B(N_\mathrm{p} + 1)}\,, \tag{7}$$

where B is given by equation (6) and

$$A = \frac{2}{(N_\mathrm{s} - N_\mathrm{b} - 1)(N_\mathrm{s} - N_\mathrm{b} - 4)}. \tag{8}$$

Taylor & Joachimi (2014) derived general formulae for the full propagation of the noise due to the finite sampling

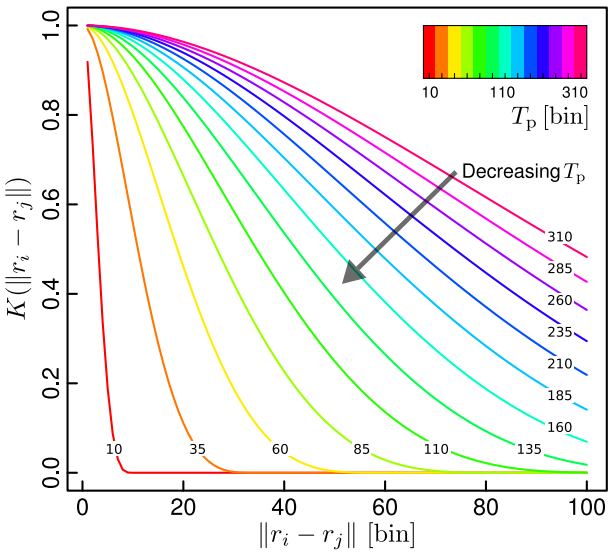


Figure 1. The behaviour of the family of tapering functions used in this work (the Wendland 2.0 function class) corresponding to different values of the tapering parameter $T_{\rm p}$. The abscissas represent the distance between two measurement locations (denoted by r_i) in data set space, which are shown in units of data ordinals (i.e bin units, $r_i \equiv i$). Larger values of $T_{\rm p}$ result in functions with a larger support interval.

of the data covariance matrix into the parameter covariance estimated from the likelihood width and peak scatter estimators, which do not coincide unless the data covariance is exactly known. Their results are in good agreement with the second-order approximations of Dodelson & Schneider (2013) and Percival et al. (2014) in the regime of $N_{\rm s} \gg N_{\rm b} \gg N_{\rm p}$, but show deviations from these results for smaller number of simulations.

In the large $N_{\rm s}$ limit, the correction factor of equation (7) can be used to obtain constraints that correctly account for the additional uncertainty due to the noise in the precision matrix estimate of equation (4). However, this additional uncertainty in the parameter covariance matrix, hinders the constraining power of the data. Given the number of bins in a measurement $\mathbf{D}$ and the number of parameters that one wishes to explore, the correction factor of equation (5) can be used to estimate the number of synthetic measurements required to reach a given target accuracy in the derived constraints. If the number of bins in a given measurement is large, as could be the case for anisotropic or tomographic clustering measurements, the required number of mock realizations to keep the additional uncertainty under control might become infeasible. The aim of our analysis is to test a new technique to reduce the impact of the uncertainties in $\hat{\mathbf{\Psi}}$ on the final parameter constraints, which could help to significantly relieve these requirements.

3 COVARIANCE TAPERING FOR LIKELIHOOD-BASED ESTIMATION

In this section we describe the covariance tapering technique developed by Kaufman et al. (2008) to improve the efficiency on the computation of MLE. This method was first applied to clustering measurements in Paz et al. (2013). The original idea behind CT is the fact that, in many applications, the correlation between data pairs far apart is negligible and little information is lost by treating these points as being independent. In this case, setting their corresponding elements in the covariance matrix to be exactly zero makes it possible to take advantage of fast numerical methods for dealing with sparse matrices, leading to a significant speed up of the evaluation of the likelihood function.

However, in this work we focus on a different use of CT. The off-diagonal elements of the covariance matrix of a general measurement might exhibit a wide range of values and uncertainties. Even when these elements are non-negligible, their relevance to obtain an accurate description of the likelihood function must be assessed in terms of their associated errors. In this way, by down-weighting the contribution of these points (which typically have a low signal to noise ratio) to the estimated precision matrix it is possible to avoid the propagation of errors into the final cosmological constraints.

Kaufman et al. (2008) define a tapered covariance matrix, $\mathbf{C}^{\rm t}$, in terms of the estimate $\hat{\mathbf{C}}$ of equation (3) and a properly defined tapering matrix $\mathbf{T}$ as

$$\mathbf{C}^{\rm t} = \hat{\mathbf{C}} \circ \mathbf{T}, \tag{9}$$

where $\circ$ indicates the Hadamard product (i.e. the entry-wise product). The Schur product theorem guaranties that if $\hat{\mathbf{C}}$ and $\mathbf{T}$ are positive definite matrices, then so is $\mathbf{C}^{\rm t}$. The tapering matrix $\mathbf{T}$ is defined as an isotropic covariance matrix by means of a taper function K as

$$T_{ij} = K(\|r_i - r_j\|), \tag{10}$$

where r_i is the i-th measurement location on the data space (e.g. the bin separation for correlation function measurements). The function K could in principle be any positive compact-support function intended to nullify the covariance matrix entries far away from the diagonal. However only certain types of functions (the Matérn class) ensure the asymptotic convergence of the method to the desired maximum likelihood estimate (see theorems 1 and 3 in Kaufman et al. 2008). Following Kaufman et al. (2008) we use the monoparametric family of functions defined by Wendland (1995, 1998)

$$K(x) = \begin{cases} \left(1 - \frac{x}{T_{\rm p}}\right)^4 \left(4\frac{x}{T_{\rm p}} + 1\right) & \text{if } x < T_{\rm p} \\ 0 & \text{if } x \geqslant T_{\rm p} \end{cases} \tag{11}$$

Fig. 1 shows the behaviour of these functions for different values of the tapering parameter, $T_{\rm p}$, which defines the size of the function support (i.e. the interval where K takes non-zero values, for more details see Kaufman et al. 2008).

As shown by Kaufman et al. (2008), the estimation of the precision matrix simply as the inverse of the tapered covariance $\mathbf{C}^{\rm t}$ can introduce systematic biases on the obtained parameter constraints. However, by applying a second Hadamard product to the inverse of $\mathbf{C}^{\rm t}$ and estimating the precision matrix as

$$\mathbf{\Psi}^{\rm t} = \left(1 - \frac{N_{\rm b} + 1}{N_{\rm s} - 1}\right) \left(\hat{\mathbf{C}} \circ \mathbf{T}\right)^{-1} \circ \mathbf{T} \tag{12}$$

it is possible to obtain an unbiased and robust estimate of the precision matrix over a large range of $T_{\rm p}$ values.

The likelihood is then estimated by replacing $\mathbf{\Psi}$ in equation 1, by the two-tapered precision matrix estimator, $\mathbf{\Psi}^{\rm t}$. In

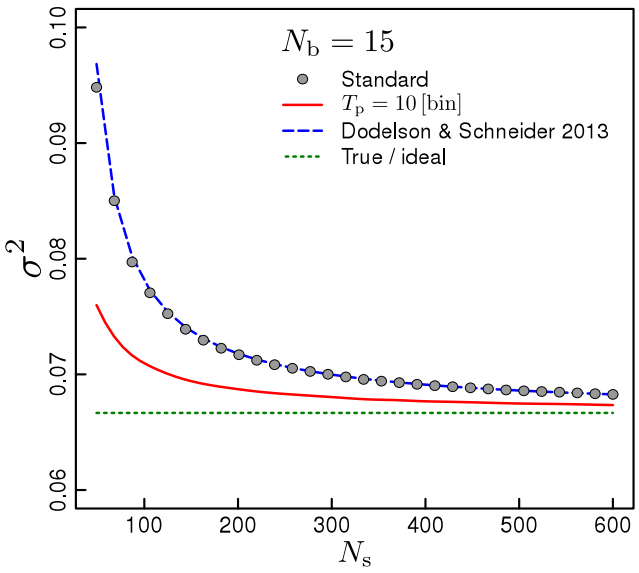


Figure 2. Variance of 10^5 MLE of the mean of sets of $N_b = 15$ uncorrelated normal random variables, as a function of the number of independent data realizations used on estimation of the precision matrix. Open symbols correspond to the variance obtained when the standard method is used (i.e. the precision matrix is approximated by $\hat{\mathbf{\Psi}}$). The dashed line shows the results obtained when applying the CT technique (i.e. the precision matrix is approximated by $\mathbf{\Psi}^t$) with a tapering parameter of 10 bins. The solid line corresponds to the analytic formulae given in Dodelson & Schneider (2013). The dotted line correspond to the expected variance for the mean of uncorrelated Gaussian random variables with first and second moment equal to zero and one, respectively.

the following sections we will show that the CT method is not only useful to approximate the MLE in a more computationally efficient way, as shown in Kaufman et al. (2008). As we will see, CT is also an appropriate technique to significantly reduce the impact of the noise in the precision matrix estimated from a set of mock measurements, increasing in this way the precision of the obtained likelihood confidence regions.

4 COVARIANCE TAPERING IN PRACTICE

4.1 Testing CT on independent normal-distributed measurements

In this section we compare the performance of the CT approach with the standard MLE method when applied to the case of N_b independent normal-distributed random variables, in a similar analysis to those performed by Dodelson & Schneider (2013); Taylor et al. (2013) and Percival et al. (2014). This simple test is able to illustrate how the CT technique can be used to minimize the effects of covariance errors on the estimation of likelihood confidence intervals.

Our data set for this test consists of N_b Gaussian numbers with null mean and standard deviation equal to unity, in which case the covariance matrix is given by the $N_b \times N_b$ identity matrix. However, we perform a MLE of the sample mean, μ, without assuming any data independence. We first compute $\hat{\mathbf{C}}$ from a set of N_s independent Monte-Carlo realizations of N_b independent Gaussian numbers D_i^s. This estimate can be used to obtain $\hat{\mathbf{\Psi}}$ and $\mathbf{\Psi}^t$ using eqs.(3) and (12). Both of these estimates will include "apparent" correlations between different bins, due to the noise in the off-diagonal elements. We generate an additional independent set of N_b Gaussian numbers to be used as the data set for the target parameter estimation. The estimation of the sample mean is achieved by maximizing the likelihood function in equation (1). In this case the model is quite simple, a constant function $T_i(\mu) = \mu$. This procedure is repeated 10^5 times, obtaining an estimation for the target parameter on each time. By using the set of all the estimated values of μ we are able to compute the standard error σ achieved by the MLE method. The use of an independent data set on parameter estimation, employing the first N_s samples for the estimation of $\hat{\mathbf{C}}$, gives an unbiased set of target parameter estimations (Percival et al. 2014).

The results of this test are shown in Fig. 2, where the open points correspond to the parameter variance obtained when the standard technique is used, i.e. the precision matrix is approximated by $\hat{\mathbf{\Psi}}$, for the case of $N_b = 15$. The comparison of these results with the dotted line, which corresponds to the true expected variance of the mean of a Gaussian random variable, illustrates the effect of the noise in the covariance matrix. As can bee seen, the variance decreases as N_s increases, which is expected due to the corresponding improvement on the $\hat{\mathbf{C}}$ estimations. This behaviour is well described by the formulae given in Dodelson & Schneider (2013), as can bee seen by looking at the dashed line in Fig. 2. The same behaviour has been seen over a wide range of N_b. The agreement found here is consistent with the results of Taylor & Joachimi (2014), given that the cases considered here correspond to the regime of large N_s compared to the number of parameters and data bins used. The solid line corresponds to the variance obtained when the precision matrix is estimated using $\mathbf{\Psi}^t$ of equation (12) with a tapering scale of 10 bins. The application of the CT method significantly reduces the impact of the noise in the variance of the target parameter, leading to results that are much closer to those of the ideal case.

4.2 Testing the CT method for realistic covariances

In the previous section we tested the results obtained by applying CT in an ideal case in which the true covariance matrix is diagonal. In this section we extend this test by considering the case in which the different elements of the dataset have non-negligible correlations. To this end, we generate Monte Carlo realizations of N_b Gaussian random variables with zero mean, correlated following a realistic model of the covariance matrix of the two-point correlation function (Sánchez et al. 2008). The upper triangular of the top-left panel of Fig. 3 shows the model for the covariance matrix for the case of $N_b = 50$, normalized as indicated in the figure key (that is, the correlation matrix). For comparison, the lower triangular part of the same panel shows the estimate $\hat{\mathbf{C}}$ obtained using 300 independent Monte Carlo realizations. As can be seen, the main features of the model covariance matrix are recovered. However the presence of noise is clear in the off-diagonal elements of the matrix, corresponding to covariances of measurements at large separations. The signal-to-noise ratio of the covariance matrix is smaller for

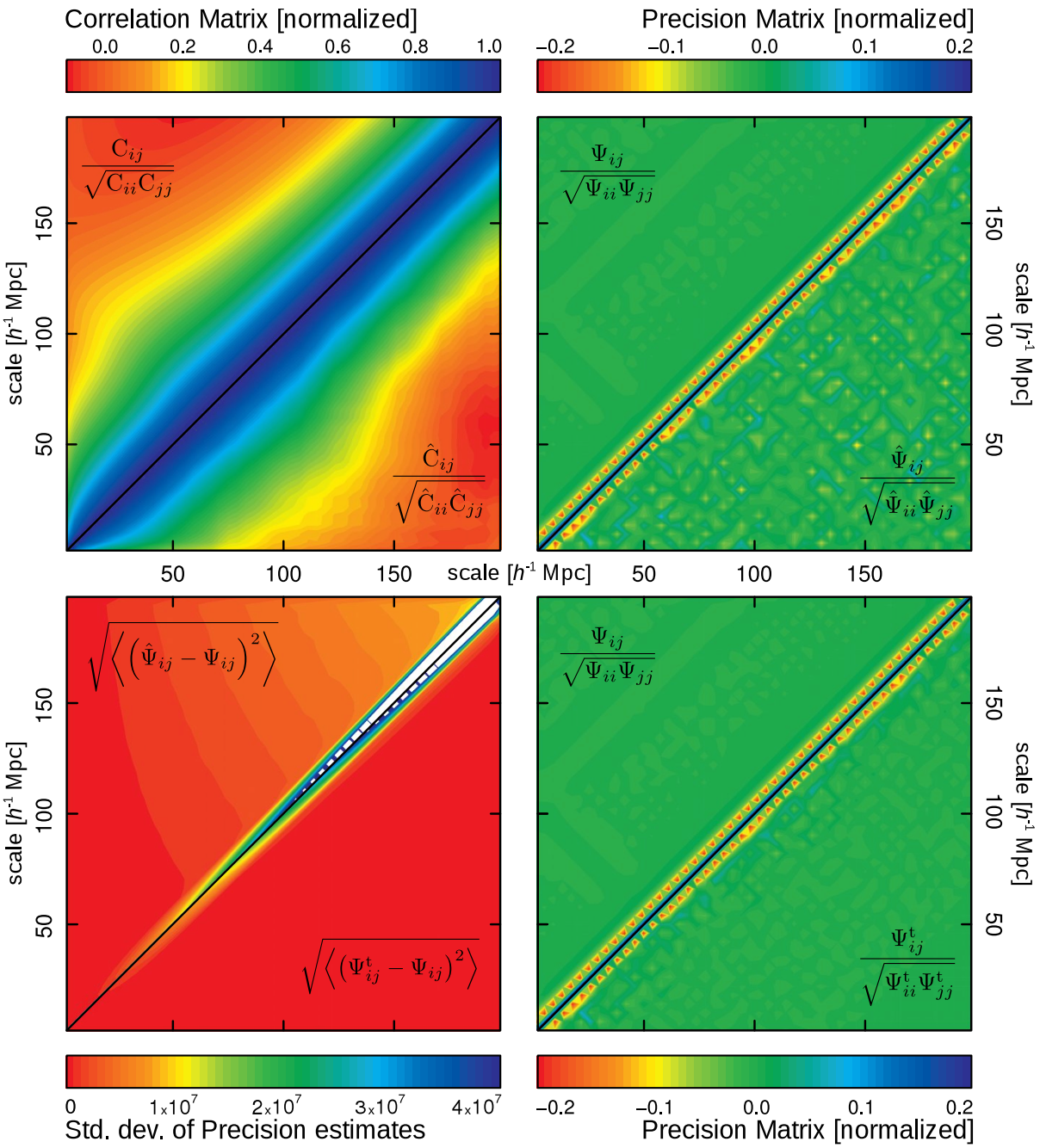


Figure 3. *Top left panel:* Comparison between the model for the covariance matrix used in this work (upper triangular part) and the standard estimation using 300 realizations. *Top right panel:* The true precision matrix $\mathbf{\Psi}$ (the matrix inverse of the model, upper triangular part) compared to the usual estimator $\hat{\mathbf{\Psi}}$. *Bottom right panel:* As in the above panel, but comparing this time $\mathbf{\Psi}$ with the CT estimator $\mathbf{\Psi}^{\rm t}$ using $T_{\rm P} = 230\,h^{-1}$Mpc. *Bottom left panel:* Standard deviations for 10^4 precision matrix estimates, with (lower triangular part) and without CT (upper triangular part), around the true matrix $\mathbf{\Psi}$.

the off-diagonal elements. The main idea of this work is to control the propagation of these errors into the precision matrix, restricting in this way their impact on the likelihood function and the obtained confidence intervals of the target parameters.

The top right panel of Fig. 3 shows the precision matrices corresponding to the model for the covariance matrix (upper triangular part) and the one obtained using the standard estimator of equation (4), normalized in analogous manner to the covariance matrices. As can be seen, the presence of noise in the off-diagonal elements is even more remarkable in the case of the precision matrix. The increment on the noise is due to the propagation of errors during the matrix inversion operation. The bottom-right panel of Fig. 3 shows a comparison of the precision matrix obtained by applying CT with a tapering parameter $T_{\rm P} = 230\,h^{-1}$Mpc (lower triangular part) and the model precision matrix (upper triangular part, identical to the one shown in the upper

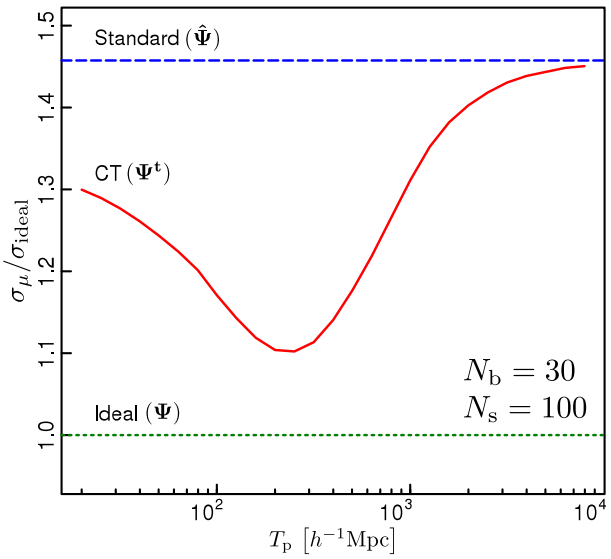


Figure 4. Error of the mean of $N_b = 30$ random Gaussian numbers with zero mean and covariance given by the model of Sánchez et al. (2008), normalized to the ideal error σ_{ideal} predicted by the model. The dashed line corresponds to the error obtained using the standard method, where the $\hat{\mathbf{\Psi}}$ estimator is taken as a proxy of the ideal precision matrix. The solid line shows the results corresponding to the CT technique, where the precision matrix is estimated by $\mathbf{\Psi^t}$. The dotted line corresponds to the ideal error.

part of the top-right panel). The application of CT leads to a significant suppression of the noise in the off-diagonal elements of the precision matrix.

The improvement in the accuracy obtained by applying CT can be quantified by computing the deviations of the different estimators from the true model precision matrix. The lower left panel of Fig. 3, shows the standard deviations, element by element, of the estimators $\hat{\mathbf{\Psi}}$ and $\mathbf{\Psi^t}$ for $N_s = 300$, with respect to the ideal precision matrix. The upper triangular part corresponds to the deviations obtained using the standard method (which are well approximated by the analytic formulae given in Taylor et al. 2013), whereas the lower triangular part shows the results obtained using the CT technique. The standard deviations obtained when CT is applied are smaller than those achieved by the standard technique, indicating a better performance at recovering the correct underlying precision matrix.

The success of the covariance tapering method depends on the selection of an adequate tapering scale T_p. In the case analysed in this section, a natural way to characterize the different approaches is through the recovered error in the mean μ. The ideal error, which represent the true constraining power of a given data set, can be easily computed by taking the inverse of the single element of the fisher matrix. As the derivative of the model with respect to the target parameter is 1 for each of the N_b dimensions, the ideal error of the mean is simply given by $\sigma_{ideal} = 1/\sum_{ij}\Psi_{ij}$. Fig. 4 shows a comparison between the standard and CT methods for a fixed number of bins and simulations ($N_b = 30$, $N_s = 100$). For each method we show the ratio $\sigma_\mu/\sigma_{ideal}$. The solid line corresponds to the results obtained by applying CT as a function of the tapering scale T_p. The dashed line shows to the error obtained using the standard method, where the precision matrix is estimated by $\hat{\mathbf{\Psi}}$. The standard deviation obtained in this case corresponds to an excess of 45% with respect to that of the ideal case, indicated by the dotted line. As can be seen, there is an optimal tapering scale of $T_p \simeq 230\,h^{-1}\mathrm{Mpc}$), for which the error obtained is only 10% larger than the ideal value. For large tapering scales, the CT method recovers the same results as the standard technique, whereas for small T_p the errors become larger again. This behaviour might be given by the relation between the tapering scale and the structure of the off-diagonal elements of the covariance matrix. For large values of T_p, the tapering procedure damps the contribution of the most off-diagonal elements of the covariance matrix, whose intrinsic values are small and are dominated by noise. As the tapering scale is reduced, the damping of the noise is more efficient and the results become more similar to those of the ideal case. However, if the tapering scale is too small, this procedure might affect entries of the covariance matrix whose intrinsic values are not small. As these off-diagonal elements are affected, the obtained results deviate again from those of the ideal case.

In Fig. 5 we show the results of extending this test to a wide range of N_s values. The variance of the MLE of the mean of 10^5 independent data sets of $N_b = 30$ correlated Gaussian numbers is shown as a function of the number of realizations employed in the estimation of $\hat{\mathbf{C}}$. The points correspond to the variance inferred using the standard technique, whereas the solid coloured lines indicate the results obtained by applying CT with different T_p values, as indicated in the figure key. The dashed line corresponds to the expected ideal variance of the mean, σ^2_{ideal}. As can bee seen in the left panel of this figure, the variance recovered by applying CT with large tapering scales is very similar to the result of the standard method. However, as the tapering scale decreases, the variance also becomes smaller, reaching values close to those of the ideal case for $T_p \simeq 230\,h^{-1}\mathrm{Mpc}$. The lower panels in Fig. 5 show the behaviour of the estimated values of the target parameter for the standard (points) and CT (solid lines) methods. In all cases the recovered values of μ show no indication of a systematic deviation from the true value $\mu = 0$, with only small fluctuations for different values of N_s.

The right panel of Fig. 5 shows the results obtained by applying the CT technique for values of the tapering scale of less than $230\,h^{-1}\mathrm{Mpc}$, which result in larger variances of the target parameter. However, it is worth noticing that even in this case there is no bias in the obtained constraints. These results suggest that the optimal tapering scale depends only on the shape of the underlying covariance matrix, rather than the number of independent data samples used to compute $\hat{\mathbf{C}}$.

5 APPLICATION TO BARYON ACOUSTIC OSCILLATION MEASUREMENT

In this section we analyse the applicability of the covariance tapering method, in the context of baryon acoustic oscillations (BAO) measurements. For this test we use the model of the full shape of the large-scale two-point correlation function, $\xi(s)$, of Sánchez et al. (2013, 2014), which is based on renormalized perturbation theory (Crocce & Scoccimarro

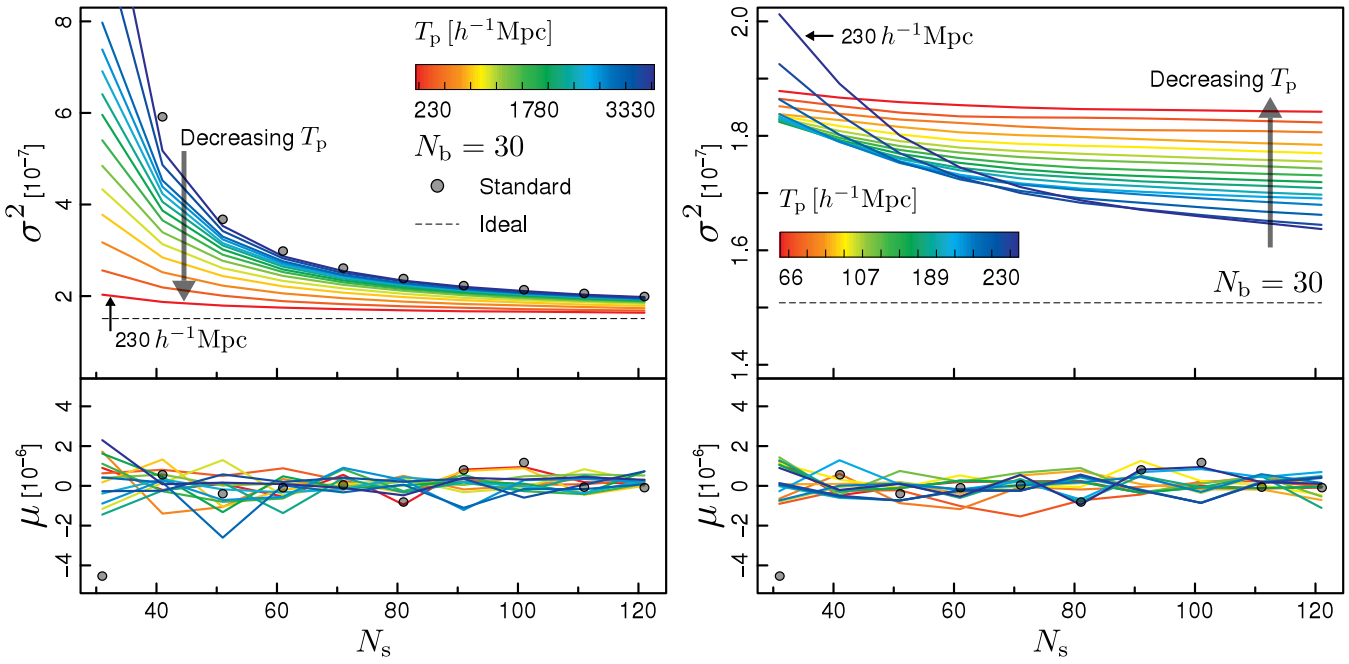


Figure 5. Variance of 10^5 MLE of the mean of N_b Gaussian numbers, following a realistic model of the covariance. The results are presented as a function of the number of samples used in the covariance estimation. Open symbols correspond to the variance obtained when the precision matrix is estimated through the standard method (i.e. $\hat{\mathbf{\Psi}} \rightarrow \mathbf{\Psi}$). Solid coloured lines show the results obtained by CT using different T_p parameter values, as indicated in the key. The dashed line correspond to the expected variance for the mean, that is the inverse of the fisher element. Left panel corresponds to T_p values between 230 and $3330\,h^{-1}$Mpc, whereas right panel shows the results of T_p ranging from 66 to $230\,h^{-1}$Mpc. The bottom subpanels at both sides show the recovered μ values for all methods.

2006). We generate sets of correlated Gaussian numbers with mean given by the model of $\xi(s)$ and the same covariance matrix as in the test of the previous section (Sánchez et al. 2008). In this way, each Monte Carlo realization mimics a realistic measurement of the correlation function at the scales relevant for BAO measurements.

As in previous sections, we generate sets of $N_{\rm s}$ random realizations of the correlation function, sampled using $N_{\rm b} = 30$ bins, varying $N_{\rm s}$ between 40 and 420. We use these synthetic samples to obtain an estimate of the covariance matrix. These realizations are analogous to the measurements from mock galaxy catalogues used to compute $\hat{\mathbf{C}}$ in most clustering analyses. We generate an additional synthetic measurement to serve as the objective data sample of the two-point correlation function, on which we perform fits of the BAO signal following the methodology of Anderson et al. (2014). More precisely, we fit the BAO peak position using a parametrization for $\xi(s)$ given by

$$\xi_{\rm mod}(s) = b^2 \xi_{\rm temp}(\alpha s) + a_0 + \frac{a_1}{s} + \frac{a_2}{s^2}, \qquad (13)$$

where $\xi_{\rm temp}(s)$ is a template given by the model of the correlation function, the parameter b corresponds to a large-scale bias factor, the shift parameter α is used to control the position of the BAO peak, and a_0, a_1 and a_2 are additional parameters used to marginalize over the broad-band signal. These fits are performed using the standard estimation of the precision matrix, $\hat{\mathbf{\Psi}}$, and the CT estimate, $\mathbf{\Psi}^{\rm t}$, with varying tapering scales. We explore the parameter space $\boldsymbol{\theta} = (\alpha, b, a_0, a_1, a_2)$ using the Markov chain Monte Carlo (MCMC) technique. We focus here on the constraints on α, marginalizing over the remaining parameters.

The procedure described above is repeated 2×10^5 times to obtain a smooth measurement of the dispersion of the α values obtained from different realizations. Fig. 6 shows the behaviour of this dispersion as a function of the number of mock samples used in the estimation of the covariance matrix. The points correspond to the results obtained when the precision matrix is approximated by the estimator $\hat{\mathbf{\Psi}}$ of equation (3). As expected, the error in α decreases as $N_{\rm s}$ increases, approaching the ideal error obtained when the true covariance matrix is used to evaluate the likelihood function, shown by the black solid line. The results from our Monte Carlo realizations are well described by the analytic formulae given by Dodelson & Schneider (2013), which is shown by the blue short-dashed line. The red long-dashed line corresponds to the result of rescaling the mean variance on α recovered from each MCMC by the correction factor of equation (7) which, as shown by Percival et al. (2014), correctly accounts for the additional error due to the noise in $\hat{\mathbf{C}}$.

The thin solid lines in Fig. 6 correspond to the results obtained using the CT method, colour-coded according to the corresponding tapering scale. For large tapering scales the results closely resemble those of the standard technique. As the tapering parameter decreases, approaching the optimal scale found in the previous section of $230\,h^{-1}$Mpc, the dispersion of the BAO scale estimates becomes closer to the ideal error. These results show that, for a given value of $N_{\rm s}$, the CT method leads to measurements of the BAO scale that are closer to the true constraining power of the data than the standard technique. For $N_{\rm s} \simeq 400$ the uncertainty

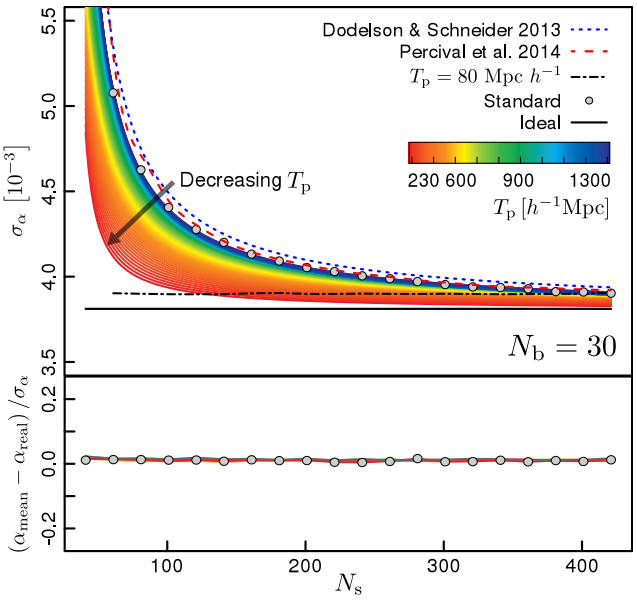


Figure 6. Standard deviation of the BAO peak scale as a function of the number of simulations used in the covariance estimate (upper panel). Open circles indicate the results corresponding to the standard method. Long and short dashed lines corresponds to the analytic formulae of Dodelson & Schneider (2013) and Percival et al. (2014). The black solid line indicates the error obtained when the ideal precision matrix is used. Coloured lines (from blue to red) show the results obtain by applying CT with different tapering scales. The black dot-dashed line show the CT results when a too small tapering parameter is used ($T_{\rm p} = 80\,h^{-1}$Mpc).

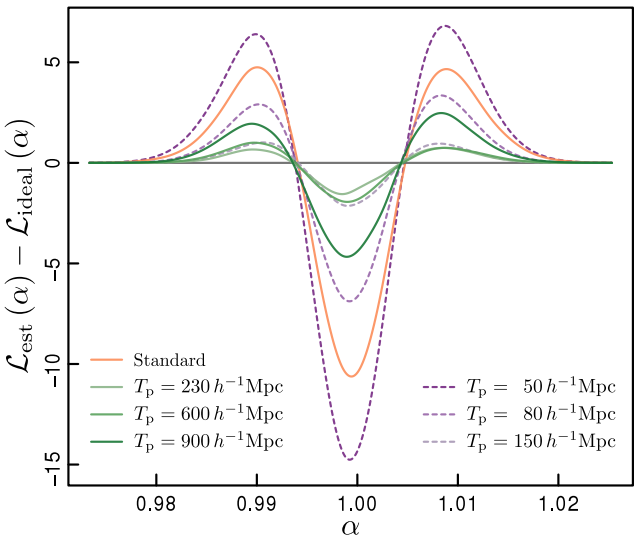


Figure 7. Difference between the mean marginalized posterior distribution of the shift parameter α obtained by applying CT with different tapering scales (green and purple lines) and that of the ideal case (gray line). The orange curve shows the results obtained by the standard method.

obtained using the CT method essentially recovers that of the ideal case.

The black dot-dashed line in Fig. 6 corresponds to the CT results obtained by setting $T_{\rm p} = 80\,h^{-1}$Mpc, illustrating the effect of implementing a too small tapering scale. As we found in the previous section, selecting a too small tapering scale leads to an increment of the errors in the target parameters. However, as shown in the lower panel of Fig. 6, even in this case the CT results show no systematic bias, with negligible differences from the true underlying parameter $\alpha_{\rm true} = 1$ for the full range of $N_{\rm s}$ values analysed.

The improvement of the constraints achieved by the CT technique with respect to the standard method ultimately relays in a closer approximation of the ideal likelihood surface. In Fig. 7 we show the difference between the mean marginalized posterior distribution of the shift parameter α obtained by applying CT with different tapering scales (green and purple lines, as indicated in the figure key) and that of the ideal case. The posterior distribution corresponding to the standard method is shown as a solid orange curve. In general, the CT results provide a closer approximation of the ideal distribution than the standard method, most notably for a tapering scale of $230\,h^{-1}$Mpc. The use of a larger tapering scale leads to larger deviations from the ideal likelihood function. However, in all of these cases they are closer to the optimal result than the standard method. In contrast, using a too small tapering scales (as in the case of $T_{\rm p} = 50\,h^{-1}$Mpc shown in the figure) leads to deviations from the underlying likelihood function that can be even larger than those obtained with the standard technique. This highlights the importance of performing a careful analysis of the optimal tapering scale for each case, which will depend on the structure of the covariance matrix.

6 SUMMARY AND CONCLUSIONS

In this work we have implemented and tested a novel technique for the estimation of the precision matrix, the covariance tapering method, developed by Kaufman et al. (2008). We have analysed the performance of the CT method and the standard technique by comparing the obtained parameter constraints with those found in the ideal case where the true precision matrix is known. For the latter case, the size of the errors in the estimated parameters is only governed by the constraining power of the data sample. Therefore, any excess seen in the recovered errors in comparison with that of the ideal case can be associated with the noise in the precision matrix estimation.

We first carried out an analysis similar to those performed by Dodelson & Schneider (2013), Taylor et al. (2013) and Percival et al. (2014), using the standard deviation of the maximum likelihood estimation of the mean of $N_{\rm b}$ independent normal random variables as a test case. Our results are in agreement with previous works, indicating that the noise in the covariance matrix estimation has a significant impact on the uncertainty obtained on parameter constraints. We found that the size of the synthetic data set used to estimate the precision matrix is crucial to control the impact of the covariance uncertainties on the final parameter constraints. Our results also show that CT helps to reduce the error in the precision matrix estimation, leading to uncertainties in the target parameters that are closer to the ideal case than those obtained with the standard method.

The efficiency of the CT technique for a data set composed of independent normal variables, where the true covariance matrix is diagonal, can be expected. In order to

check the validity of the CT method in a more realistic situation, we also studied the case of the MLE of the mean of Gaussian numbers with non-zero correlations given by a realistic model of the covariance matrix of the two-point correlation function (Sánchez et al. 2008). Our results show that also in this case the covariance tapering method leads to smaller errors than the standard technique, without introducing any systematic bias in the estimated parameters. In this case we found an optimal tapering scale, defined as the value of the tapering parameter for which the obtained standard deviation is closer to its ideal value. For example, in the case of 30 normal distributed values and 100 synthetic samples on the covariance estimation, the CT method with the optimal tapering scale, gives a standard deviation only 10% larger than that of the ideal case, whereas the standard technique results in errors 45% larger. We showed that the optimal tapering parameter depends only on the structure of the underlying covariance matrix and is insensitive to the bin size or the number of synthetic samples used in the estimation of the precision matrix. Smaller tapering parameters than the optimal value result in an increase of the standard deviation, although no bias is introduced.

Finally, we performed an analysis of the CT technique on a more realistic context by testing its applicability to isotropic BAO measurements. We used an accurate model of the large-scale two-point correlation function (Sánchez et al. 2013) and its full covariance matrix (Sánchez et al. 2008) to generate Monte Carlo realizations of this quantity. We used these synthetic measurements to perform fits of the BAO signal following the methodology of Anderson et al. (2014). We found that the CT method significantly reduces the impact of the noise in the precision matrix on the obtained errors in the BAO peak position without introducing any systematic bias. As in the previous case, the optimal tapering parameter only depends on the shape of the true covariance matrix, with a preferred $T_{\rm p}$ scale similar to that of the previous test (i.e. the case of zero-mean correlated Gaussian numbers).

Covariance tapering can help to reduce the required number of mock catalogs for the analysis of current and future galaxy surveys. This can be clearly illustrated by extending the analysis of section 5 to the case of $N_{\rm s} = 600$, corresponding to the number of mock catalogues used in the analysis of the SDSS-DR9 BOSS clustering measurements of Anderson et al. (2012). In this case, the uncertainty in the BAO shift parameter obtained by applying the CT technique is equivalent to that derived with the standard method using $N_{\rm s} = 2300$ instead.

As we highlighted before, the performance of the CT technique ultimately depends on the structure of the underlying covariance matrix. In this work we assumed a Gaussian model for the covariance matrix of the correlation function. Although this model gives an excellent description of the results of numerical simulations, more accurate models must include also the contribution from modes larger than the survey size (de Putter et al. 2012) or non-Gaussian terms (Scoccimarro et al. 1999) that would affect the off-diagonal elements of the covariance matrix. We leave the study of the performance of the CT under the presence of these contributions for future work, as well as the extension of the present analysis to alternative data sets such as the power spectrum or anisotropic clustering measurements in general.

The covariance tapering technique can be extremely useful for the analysis of future surveys such as Euclid and DESI. The small statistical uncertainties associated with these data sets will provide strong tests for the standard ΛCDM cosmological model. However the large number of mock catalogues that are required by the standard technique to maintain the accuracy level of the cosmological constraints might be infeasible. The application of the covariance tapering technique can significantly reduce the number of mock catalogues required for the analysis these surveys, allowing them to reach their full constraining power.

ACKNOWLEDGMENTS

The authors are thankful to Andrés Nicolás Ruiz and Salvador Salazar-Albornoz for useful discussions and suggestions about this manuscript. DJP acknowledges the support from Consejo Nacional de Investigaciones Científicas y Técnicas de la República Argentina (CONICET, project PIP 11220100100350) and the Secretaría de Ciencia y Técnica de la Universidad Nacional de Córdoba (SeCyT, project number 30820110100364). DJP also acknowledges the hospitality of the Max-Planck-Institut für extraterrestrische Physik were part of this work was carried out. AGS acknowledges the support from the Trans-regional Collaborative Research Centre TR33 'The Dark Universe' of the German Research Foundation (DFG).

REFERENCES

Anderson L. et al., 2014, MNRAS, 441, 24
Anderson L. et al., 2012, MNRAS, 427, 3435
Chuang C.-H., Kitaura F.-S., Prada F., Zhao C., Yepes G., 2015, MNRAS, 446, 2621
Crocce M., Scoccimarro R., 2006, Phys. Rev. D, 73, 063519
de Putter R., Wagner C., Mena O., Verde L., Percival W. J., 2012, JCAP, 4, 19
Dodelson S., Schneider M. D., 2013, Phys. Rev. D, 88, 063537
Eisenstein D., DESI Collaboration, 2015, in American Astronomical Society Meeting Abstracts, Vol. 225, American Astronomical Society Meeting Abstracts, p. 336.05
Hartlap J., Simon P., Schneider P., 2007, A&A, 464, 399
Kalus B., Percival W. J., Samushia L., 2015, ArXiv e-prints
Kaufman C. G., Schervish M. J., Nychka D. W., 2008, J. Am. Statist. Assoc., 15451555
Kaufman G. M., 1967, Center for Operations Research and Econometrics Report, No. 6710
Kitaura F.-S., Yepes G., Prada F., 2014, MNRAS, 439, L21
Koda J., Blake C., Beutler F., Kazin E., Marin F., 2015, ArXiv e-prints
Laureijs R. et al., 2011, ArXiv e-prints
Manera M. et al., 2014, in IAU Symposium, Vol. 306, IAU Symposium, pp. 266–268
Manera M. et al., 2013, MNRAS, 428, 1036
Monaco P., Theuns T., Taffoni G., 2002, MNRAS, 331, 587
Paz D., Lares M., Ceccarelli L., Padilla N., Lambas D. G., 2013, MNRAS, 436, 3480
Percival W. J. et al., 2014, MNRAS, 439, 2531
Planck Collaboration et al., 2015, ArXiv e-prints

Sánchez A. G., Baugh C. M., Angulo R. E., 2008, MNRAS, 390, 1470
Sánchez A. G. et al., 2013, MNRAS, 433, 1202
Sánchez A. G. et al., 2014, MNRAS, 440, 2692
Scoccimarro R., Zaldarriaga M., Hui L., 1999, ApJ, 527, 1
Tassev S., Zaldarriaga M., Eisenstein D. J., 2013, JCAP, 6, 36
Taylor A., Joachimi B., 2014, MNRAS, 442, 2728
Taylor A., Joachimi B., Kitching T., 2013, MNRAS, 432, 1928
Wendland H., 1995, Advances in computational Mathematics, 4, 389
Wendland H., 1998, Journal of approximation theory, 93, 258
Wishart J., 1928, Biometrika, 32